Title

Ferumoxytol: a new, clinically applicable label for stem-cell tracking in arthritic joints with MRI

Journal

Nanomedicine, 8(12)

ISSN

1743-5889

Authors

Khurana, Aman
Nejadnik, Hossein
Chapelin, Fanny
et al.

Publication Date

2013-12-01

DOI

10.2217/nnm.12.198

Peer reviewed

Published in final edited form as:
Nanomedicine (Lond). 2013 December ; 8(12): . doi:10.2217/nnm.12.198.

Ferumoxytol: a new, clinically applicable label for stem-cell tracking in arthritic joints with MRI

Aman Khurana[‡,1], **Hossein Nejadnik**[‡,1], **Fanny Chapelin**[1], **Olga Lenkov**[1], **Rakhee Gawande**[1], **Sungmin Lee**[2], **Sandeep N Gupta**[3], **Nooshin Aflakian**[1], **Nikita Derugin**[1], **Solomon Messing**[4], **Guiting Lin**[5], **Tom F Lue**[5], **Laura Pisani**[1], and **Heike E Daldrup-Link**[*,1]

[1]Department of Radiology & Molecular Imaging Program at Stanford, Stanford University, Stanford, CA, USA

[2]Department of Electrical Engineering, Stanford University, Stanford, CA, USA

[3]Biomedical Image Analysis Laboratory, GE Global Research, Niskayuna, NY, USA

[4]Department of Communication & Statistics, Stanford University, Stanford, CA, USA

[5]Department of Urology, University of California San Francisco, CA, USA

Abstract

Aim—To develop a clinically applicable MRI technique for tracking stem cells in matrix-associated stem-cell implants, using the US FDA-approved iron supplement ferumoxytol.

Materials & methods—Ferumoxytol-labeling of adipose-derived stem cells (ADSCs) was optimized *in vitro*. A total of 11 rats with osteochondral defects of both femurs were implanted with ferumoxytol- or ferumoxides-labeled or unlabeled ADSCs, and underwent MRI up to 4 weeks post matrix-associated stem-cell implant. The signal-to-noise ratio of different matrix-associated stem-cell implant was compared with *t*-tests and correlated with histopathology.

Results—An incubation concentration of 500 μg iron/ml ferumoxytol and 10 μg/ml protamine sulfate led to significant cellular iron uptake, T2 signal effects and unimpaired ADSC viability. *In vivo*, ferumoxytol-and ferumoxides-labeled ADSCs demonstrated significantly lower signal-to-noise ratio values compared with unlabeled controls ($p < 0.01$). Histopathology confirmed engraftment of labeled ADSCs, with slow dilution of the iron label over time.

Conclusion—Ferumoxytol can be used for *in vivo* tracking of stem cells with MRI.

Keywords

iron oxide nanoparticle; matrix-associated stem-cell implant; MRI osteoarthritis; stem-cell tracking

[*]Author for correspondence: Tel.: +11 650 723 8996, h.e.daldrup-link@stanford.edu.
[‡]Authors contributed equally

Financial & competing interests disclosure
The authors have no other relevant affiliations or financial involvement with any organization or entity with a financial interest in or financial conflict with the subject matter or materials discussed in the manuscript apart from those disclosed.
No writing assistance was utilized in the production of this manuscript.

Ethical conduct of research
The authors state that they have obtained appropriate institutional review board approval or have followed the principles outlined in the Declaration of Helsinki for all human or animal experimental investigations. In addition, for investigations involving human subjects, informed consent has been obtained from the participants involved.

Arthritis is one of the most common causes of disability, affecting approximately 49.9 million individuals in the USA, and resulting in 44 million outpatient visits, 992,100 hospitalizations, US$95 billion direct costs for medical treatment and US$47 billion in indirect costs due to lost earnings [1, 2] . A major challenge in the treatment of cartilage defects due to arthritis is the lack of self-regeneration capacity of the injured cartilage [3, 4] . New therapies based on matrix-associated chondrocyte implants or matrix-associated stem-cell transplants (MASIs) provide a potentially curative therapeutic option [5–10] .

A major barrier for evaluations of the long-term success of engraftment outcomes of different matrix-associated chondrocyte implant and MASI approaches is the current inability to recognize complications of the engraftment process in a timely manner. Complications in the early post-transplant period include loss of stem cells from the transplantation site due to mechanical loss and/or apoptosis [11, 12] . An imaging method that could visualize and monitor the presence of stem cells in MASIs directly, noninvasively and longitudinally *in vivo* would greatly enhance the ability to develop more successful cartilage regeneration techniques.

Superparamagnetic iron oxide nanoparticles (SPIOs) provide a strong signal effect on magnetic resonance (MR) images and can be internalized into stem cells. MRI is currently the only noninvasive diagnostic test that can provide high-resolution anatomical and functional information of cartilage defects *in vivo* [5,13–16]. A variety of iron oxide nanoparticle-based stem-cell markers have been previously applied for cell-tracking purposes [15, 17–21] . However, these previously applied cell labels are either not clinically applicable or have been taken off the market [22–24] . The authors propose to utilize the US FDA-approved iron supplement ferumoxytol (Feraheme®, Advanced Magnetics, MA, USA) for stem-cell labeling. This agent is currently used for the treatment of iron deficiency [25] in patients with anemia. Ferumoxytol provides a strong signal on MR images. Thus, the authors hypothesized that this clinically applicable iron oxide nanoparticle compound could be also used as a stem-cell marker [20] . To the best of the authors' knowledge, ferumoxytol is currently the only iron oxide nanoparticle compound that could be directly translated to the clinic and applied for stem-cell MRI in patients via an 'off-label' use.

Thus, the goal of this study was to develop an immediately clinically applicable MRI test for *in vivo* tracking of MASIs based on ferumoxytol-labeling of the transplanted stem cells. By exploiting this novel, immediately clinically applicable cell-tracking technique as a new tool to monitor stem-cell engraftment outcomes noninvasively *in vivo*, the authors anticipate significantly facilitating the development of successful therapies for cartilage regeneration in patients.

Materials & methods

Adipose-derived stem cells

Adipose-derived stem cells (ADSCs) have been recently introduced as a new source for MASIs. Subcutaneous adipose depots, the source for these cells, are abundant and easily accessible, thereby providing a potentially unlimited ADSC reservoir. ADSCs demonstrate similar chondrogenic differentiation outcomes when compared with mesenchymal stem cells (MSCs), which are typically harvested from bone marrow aspirations or biopsies [26–29]. Considering these factors, ADSCs have become an attractive alternative source of stem cells for MASI. ADSCs for this study (generous gift from G Lin and T Lue, University of California, San Francisco, CA, USA) were obtained from male Sprague–Dawley rats as previously described by Ning *et al.* [30] . Like MSCs, ADSCs express CD29, CD44, CD71, CD90, CD105/SH2, SH3 and the widely recognized stem-cell marker STRO-1. ADSCs do not express CD31, CD45 and CD106 [30–32] . The hematopoietic cell marker CD34 is

present in early, but not late, passages [30,33]. The lack of CD106 on ADSCs is consistent with the origin of these cells from nonhematopoietic tissue [32] . ADSCs were cultured in DMEM (Invitrogen, CA, USA) supplemented with 10% fetal bovine serum (FBS; Invitrogen), 100 U/ml pencillin and 100 μg/ml streptomycin (Invitrogen) at 37°C in a humidified 5% CO_2 atmosphere. At 90% confluency, the ADSCs were trypsinized and either redistributed to new culture flasks or used for experiments.

Contrast agents

Ferumoxytol (Feraheme) is an iron supplement that has been FDA approved for intravenous treatment of iron deficiencies in patients with renal failure [25]. Feraheme nanoparticles have a mean hydrodynamic diameter of 20–30 nm and are composed of an iron oxide core (diameter of 6.76 nm ± 0.41) and a hydrophilic carboxydextran coat [34]. The superparamagnetic nanoparticles have a strong signal effect on T1- and T2-weighted MR images, reflected by an r1 relaxivity of 38 mM^{-1} s^{-1} and an r2 relaxivity of 83 mM^{-1} s^{-1} at 20 MHz (0.47 T) [20].

As a standard of reference for MR signal effects of ferumoxytol, FDA-approved SPIOs, ferumoxides (Endorem®, Guerbet, Aulnaysous-Bois, France and Feridex I.V. ®, Bayer Healthcare, NJ, USA) were used, which have been extensively applied for cell-labeling and cell-tracking purposes [15,17–21] . However, ferumoxides have been recently taken off the market by the pharmaceutical companies and no longer available. Ferumoxides nanoparticles are composed of an iron oxide core (5–30 nm) and a dextran coat. Ferumoxides nanoparticles have a hydrodynamic diameter of 120–180 nm, and a r1 relaxivity of 40 mM^{-1} s^{-1} and an r2 relaxivity of 160 mM^{-1} s^{-1} at 0.47 T at 37°C [35] .

Stem-cell labeling

ADSCs were labeled with ferumoxytol and protamine sulfate (American Pharmaceuticals Partners, IL, USA) using a labeling technique adapted from previous techniques described by Arbab *et al.* [36, 37] . To optimize the ferumoxytol-labeling protocol, samples of 0.5×10^6 ADSCs were incubated with labeling media, consisting of increasing concentrations of 0, 100, 200, 300, 400, 500 and 700 μg iron/ml ferumoxytol and 10 μg/ml protamine sulfate. Serum-free ferumoxytol–protamine complex(ed) labeling media was prepared by incubation of ferumoxytol with protamine sulfate at the aforementioned concentrations in serum-free DMEM for 5 min to allow for complex formation based on a recent published technique from the authors' laboratory [38]. Cell samples were incubated with this serum-free labeling media for 4 h. Then, 10% FBS was added and cells were further incubated overnight at 37°C and 5% CO_2.

Initial results (see below) demonstrated that a concentration of 500 μg iron/ml ferumoxytol and 10 μg/ml protamine sulfate provided maximal ferumoxytol uptake and MR signal effects without impairment in ADSC viability. Cells labeled with this concentration were used for *in vitro* and *in vivo* MRI studies.

For comparison, control ADSCs were labeled with ferumoxides via simple incubation using established labeling protocols in the authors' laboratory [15,17,19]. In total, 0.5×10^6 ADSCs were incubated with 100 μg iron/ml ferumoxides in serum-free media for 4 h, followed by an incubation in FBS-supplemented media overnight at 37°C and 5% CO_2. Comparisons with recently published Thu *et al.*'s technique were also performed as per their published method [39] .

After completion of incubation procedures, all cell samples were washed three times with phosphate-buffered saline by sedimentation (at 25°C at 1000 rpm for 5 min), resuspended in DMEM and used for *in vitro* or *in vivo* investigations.

In vitro studies

Triplicate samples of 0.5×10^6 ADSCs, labeled with different concentrations of ferumoxytol as described above, were transferred to test tubes, dissolved in 10 µl agarose (4%; Type VII, Sigma-Aldrich, MO, USA) and placed in a waterbath to avoid artefacts from surrounding air. All cell samples underwent MRI on a 7 T MR scanner (MicroSigna 7.0; General Electric, NY, USA) using a custom-built single-channel transmit/receive partial birdcage (internal diameter: 3 cm) radiofrequency (RF) coil for high-resolution MRI.

Sagittal MR images of the cell samples were obtained with a fast spin echo sequence (repetition time: 3000 ms, echo time: 30 ms) and a multiecho spin echo sequence (repitition time: 4000 ms/echo time: 15, 30, 45 and 60 ms). All MR images were obtained with a feld-of-view of 3.5 × 3.5 cm, a matrix of 256 × 256 pixels, a slice thickness of 0.5 mm and a number of excitations of 16. Operator-defined regions of interest were used to determine the mean signal intensity (SI) of each sample on the multiecho spin echo images. T2 relaxation times and T2 maps were calculated by Cine Tool (GE Global Research, NY, USA) based on the data from the multiecho spin echo images for each concentration of ferumoxytol.

Cell viability—The viability of the cell samples was determined 24-h post labeling and just before implantation in the MASI by the trypan blue exclusion test. Labeled ADSCs as well as nonlabeled controls were exposed to trypan blue and the relative number of nonstained, viable cells to the number of stained, nonviable cells was calculated with the use of an automatic cell counter (Countess® Automated Cell Counter, Invitrogen).

Spectrometry—The iron concentration within all test samples was determined with inductively coupled plasma optical emission spectrometry. The samples were mineralized with metal-free hydrochloric acid (Fischer Scientific, ON, Canada) overnight and the obtained solutions were nebulized into an argon plasma. Spectrometric analyses were performed by collaborators at the Environmental Measurement 1: Gas–Solution Analytical Center at Stanford (CA, USA), who were blinded with regard to the content of the samples.

Histopathology—Triplicate samples of ferumoxytol-labeled and unlabeled cells were stained with the Accustain™ Prussian blue kit (Sigma-Aldrich) and post-3,3´-diaminobenzidine (DAB) enhancement with the SIGMA *FAST*™ DAB with Metal Enhancer kit (Sigma-Aldrich). For further confirmation of intracellular compartmentalization of the applied iron oxide nanoparticles, cells were labeled with fluorescein isothiocyanate-conjugated ferumoxytol and imaged on a Cell-IQ® 2 imager, using Imagen 2.6.0 and Analyser 3.0.1 software (Chip-Man Technologies Ltd, Tempere, Finland). The fluorescent signal of labeled cells and unlabeled controls was recorded and evaluated for significant differences using *t*-test with a significance level of $p < 0.05$.

Chondrogenic differentiation—Both labeled ADSCs (with 500 µg/ml ferumoxytol and 10 µg/ml protamine sulfate) and unlabeled controls were detached and centrifuged at 1000 rpm for 5 min. In total, 2.5×10^5 cells were resuspended in 0.5 ml of serum-free chondrogenic differentiation media (consisting of KnockOut™ DMEM/F-12 [Life Technologies, CA, USA], 100 U/ml penicillin, 100 µg/ml streptomycin [Gibco, NY, USA], 1% GlutaMAX™ [Life Technologies], 50 µg/ml L-ascorbic acid 2-phosphate sequimagnesium [Sigma-Aldrich], 100 µg/ml sodium pyruvate [Gibco], 40 µg/ml L-proline [Sigma-Aldrich], 100 nM dexamethasone [Sigma-Aldrich], ITS™ + Premix (BD, MA, USA) final concentration: 5.5 µg/ml transferrin, 10 µg/ml bovine insulin, 5 µg/ml sodium selenite, 4.7 µg/ml linoleic acid and 500 µg/ml bovine serum albumin [BD Bioscience, NJ, USA] and 10 ng/ml TGF-β3 [R&D Systems, MN, USA]), and centrifuged again at 1000 rpm for 5 min. Cells were kept as a pellet and the media was changed every 2 days.

At 2 weeks, the pellets were fixed in formalin (10%; BDH, PA, USA) and the same for xylene (EMD Millipore, Darmstadt, Germany). The pellets were then embedded in paraffin and sliced into 5-μm-thick tissue slices on glass slides. The slides were de-waxed and hematoxylin and eosin (H&E) and Alcian blue staining were performed.

Transmission electron microscopy—Samples (labeled and unlabeled ADSCs) were embedded in gelatin (10%) and fixed in Karnovsky's fixative: 2% glutaraldehyde (Cat. No. 16000, Electron Microscopy Sciences, PA, USA) and 4% pFormaldehyde (Cat. No. 15700, Electron Microscopy Sciences) in 0.1 M sodium cacodylate (Cat. No. 12300, Electron Microscopy Sciences) pH 7.4 for 1 h at room temperature (RT). Samples post fixed in 1% osmium tetroxide (Cat. No. 19100, Electron Microscopy Sciences) were cut into 1 mm^3 pieces and left for 1 h at RT, washed three times with ultrafiltered water, then *en bloc* stained at 4°C overnight. Samples were then dehydrated in a series of ethanol (50, 70 and 95%) xwashes for 15 min each at 4°C, then followed by two washes of 100% ethanol at RT and one wash of acetonitrile for 15 min. Samples were infiltrated with EMbed 812 resin (Cat. No.1 4120, Electron Microscopy Sciences) mixed 1:1 with acetonitrile for 2 h followed by two parts EMbed 812 to one part acetonitrile for 2 h. The samples were then placed into EMbed 812 for 2 h then placed into molds and filled with resin. The samples were then placed into a 65°C oven overnight to polymerize.

Samples were trimmed and sectioned between 75- and 90-nm thickness on a Leica Ultracut S (Leica, Wetzlar, Germany), picked up on formvar/carbon-coated slot grids (Cat. No. FCF2010-Cu, Electron Microscopy Sciences) or 100 mesh Cu grids (Cat. No. FCF100-Cu, Electron Microscopy Sciences). Grids were contrast stained for 30 s in 1:1 saturated uranylacetate (~7.7%) to 100% ethanol followed by staining in 0.2% lead citrate for 30 s. Cells were imaged on the JEOL JEM-1400 transmission electron microscope (JEOL Ltd, Tokyo, Japan) at 120 kV and photos were taken using an ORIUS™ SC200 digital camera (Gatan Inc., CA, USA).

In vivo studies

ADSC transplantation—The study was approved by the institutional animal care and use committee. In eleven nude athymic female Harlan rats, cartilage defects were created in the distal femur of both knee joints under inhalation anesthesia with 1.5–2% isoflurane in 2 l of oxygen. A medial patellar skin incision was made, the patella was dislocated laterally and a circular osteochondral defect (diameter: 2 mm, depth: 1.5 mm) was created in the distal femoral trochlear groove using a microdrill (Ideal, IL, USA). In these defects, either 7.5×10^5 ferumoxytol-labeled ADSCs (right femur: n = 7), ferumoxides-labeled ADSCs (right femur: n = 4) or unlabeled ADSCs (left femur: n = 11) were implanted, using an agarose scaffold (5 μl, Type VII). The implant location and consistency was confirmed visually. After allowing agarose (4%) to harden (1–2 min), the patella was repositioned and the skin incision was closed by Dermalon™ 6-0 monofilament sutures (Covidien, MA, USA).

MRI—Ten rats underwent MRI at the day of ADSC implantation and follow-up MR scans at 2 and 4 weeks after ADSC implantation. One additional rat with implants of ferumoxytol-labeled cells underwent MRI on the day of ADSC implantation and at 2 weeks, and was sacrificed directly after the 2-week scan to obtain histopathologic correlations of imaging data at this time point.

MRI of all knee joints was performed with the same 7 T MR scanner and RF coil used for *in vitro* studies. Animals were anesthetized with 2% isoflurane and placed supine on a custom-built trough with their knees centered in the RF coil. Sagittal MR images of the rat knee joints were obtained with a fast spin echo sequence (repetition time: 3000 ms; echo time: 30

ms; number of excitations: 16; field of view: 2.5 cm; matrix: 256 × 256 pixels; slice thickness: 0.5 mm).

MR images were analyzed using a DICOM-dedicated image processing software (OsiriX, Pixmeo, Geneva, Switzerland). The SI of the stem-cell transplant and the SI of background noise in front of the knee joint (phase-encoding direction) were measured by operator-defined regions of interest. The signal-to-noise ratio (SNR) of labeled and unlabaled MASI was calculated as: $SNR = SI_{TRANSPLANT}/SI_{NOISE}$ [40].

Histopathology—Animals were sacrificed at 2 weeks (n = 1) or at 4 weeks after ADSC implantation (n = 10). The knee joints were explanted, dissected and placed in Cal-Ex II (Fisher Scientific, NJ, USA) for 48–72 h. Cal-Ex II is a mixture of formaldehyde and formic acid that fixes and decalcifies the tissue simultaneously. The specimens were then dissected parasagitally, dehydrated through graded alcohol washes, embedded in paraffin, cut in 5-μm sections and stained with standard H&E to define the morphology of the implant. DAB–Prussian blue (Sigma-Aldrich) stains, performed on deparaffinized sections similar to *in vitro* studies (see above) were used to detect iron oxide nanoparticles. Anti-CD68 staining specific for ED-1 macrophages (primary antibody: mouse anti-rat CD68, Abcam, MA, USA; secondary antibody: Alexa Fluor® 488 Goat Anti-mouse, Invitrogen, OR, USA) was added on 2- and 4-week time points to detect any macrophage infiltration in and around the defect. FISH was performed using a rat Y-chromosome probe (ID Labs, Ontario, Canada) to detect transplanted male rat ADSCs in female rat knees.

Statistical analyses

Quantitative data of cell samples incubated with different iron oxide concentrations and evaluated at different time points after labeling were compared using *t*-tests. SNR data of MASI with iron oxide-labeled and unlabeled ADSCs were tested for significant differences with *t*-tests. Within each '*in vivo*' group, changes in SNR data over time were compared with an analysis of variance (ANOVA). *t*-tests and ANOVA models were computed using the *t*-test and aov functions in R Foundation for Statistical Computing, Vienna, Austria. Since right and left knees of each rat contained different MASI (right knee: labeled ADSCs, left knee: unlabeled ADSCs), the authors assumed that MR scans of each rat's knee were independent observations. In order to exclude that data from the same rats were dependent (e.g., different rats metabolized the iron oxide labels at different rates), multilevel models were fit to SNR data using the R package 'lme4' version 0.999375-39 with specifications identical to each repeated ANOVA. A variable that identified each rat was added as a random effect to a second model, and the fit of each model was compared. In each case, the model fits were not significantly different. For all analyses, a p-value of less than 0.05 was considered to indicate significant differences between different experimental groups or different time points of observation.

Results

Ferumoxytol labeling of ADSC leads to significant MR signal effects *in vitro*

All ferumoxytol-labeled ADSCs demonstrated a strong negative (dark) signal on T2-weighted MR images (Figure 1). Corresponding quantitative T2 relaxation times of ferumoxytol-labeled ADSCs were significantly shortened (equaling a higher MR signal effect) compared with unlabeled controls ($p < 0.05$; Figure 2). There was no significant difference in MR signal effects of ADSCs labeled with ferumoxytol concentrations below 400 μg/ml and above 500 μg/ml ($p > 0.05$). T2 times at both 400 and 500 μg/ml concentrations were significantly different from lower concentrations ($p = 0.0019$, Figure 2). Direct comparisons with Thu *et al.*'s technique (Figure 3) significantly demonstrated lower

T2 relaxation times 24-h post labeling than this study's technique (Thu *et al.*'s : 7.09 ± 1.02 ms; this study's: 11.32 ± 1.14 ms, $p < 0.05$). However, follow-up studies at 14 days after labeling revealed no significant difference in T2 relaxation values for both techniques (Thu *et al.*'s: 25.06 ± 0.77 ms; this study's: 25.4 ± 0.81 ms, $p > 0.05$).

Cell viability—ADSC labeled with ferumoxytol concentrations of 100–500 μg/ml did not show significant differences in viability compared with unlabeled controls ($p > 0.05$; Figure 2). However, after incubation with high concentrations (600–700 μg/ml), ADSC viability decreased with borderline significance compared with unlabeled controls ($p = 0.053$; Figure 2)

Cellular iron uptake—All ferumoxytol-labeled ADSCs demonstrated a significantly higher iron content compared with unlabeled controls ($p < 0.05$). Exposure of ADSCs to increasing ferumoxytol concentrations of 100–500 μg iron/ml led to a steadily increasing iron uptake, followed by a plateau at further increased concentrations (Figure 2).

Histopathology and transmission electron microscopy: DAB–Prussian blue staining and fluorescence microscopy confirmed intracellular iron uptake (Figures 4A, 4B, 4D & 4E). ADSCs labeled with fluorescein isothiocyanate-linked ferumoxytol nanoparticle showed intracellular fluorescence on fluorescence microscopy (Chip-Man Technologies Ltd) with significantly higher fluorescence compared with unlabeled controls ($p < 0.05$; Figure 4F).Transmission electron microscopy showed iron nanoparticles within secondary lysosomes of the labeled cells (arrows, Figure 4C). Chondrogenic differentiation experiments revealed unimpaired chondrogenesis of labeled cells with positive Alcian blue stains for both labeled and unlabeled cells (Figure 5).

Taken together, a labeling protocol with 500 μg iron/ml ferumoxytol and 10 μg/ml protamine sulfate was considered the best compromise between significant MR signal, maximal iron uptake and preserved viability of labeled ADSCs with uninhibited chondrogenesis. This protocol was used for subsequent *in vivo* experiments.

Ferumoxytol-labeled ADSCs can be detected *in vivo* with MRI MRI

Ferumoxytol-labeled MASI demonstrated a marked, negative signal on T2-weighted MR images (Figure 6A). The MR signal characteristics of ferumoxytol-labeled MASIs were similar to ferumoxides-labeled MASIs (Figure 6B). Unlabeled MASIs, on the other hand, demonstrated a relatively high signal on T2-weighted MR scans (Figure 6C). The T2 signal of ferumoxytol-labeled MASIs slowly increased over time while the T2 signal of unlabeled MASIs slightly decreased over time (Figures 6 & 7).

Corresponding SNR data showed significant differences between labeled and unlabeled MASIs directly after the surgery ($p < 0.01$), and at 2 weeks after MASI ($p < 0.05$; Figure 7). There was no significant difference in SNR data of ferumoxytol- and ferumoxides-labeled MASIs. At 4 weeks, SNR data of labeled ADSCs (both ferumoxytol and ferumoxides) were not significantly different compared with the unlabeled controls ($p > 0.05$; Figure 7).

Histopathology—H&E and FISH stains of MASI demonstrated engraftment of ADSC in osteochondral defects (Figures 8A–8F). There was no apparent difference between ferumoxytol- and ferumoxides-labeled and unlabeled ADSC transplants. DAB–Prussian blue showed positive staining for iron oxide nanoparticles at 2 weeks after implantation of labeled cells, which corresponded to MRI data (Figure 9A). Ferumoxytol was not detectable any more at 4 weeks post MASI, presumably due to dilution of the iron oxide label (Figure 9B). Control transplants of unlabeled cells did not show positive staining with DAB–Prussian blue (Figure 9C). No positive CD68 staining was seen in labeled and control

transplants suggesting no macrophage infiltration in the transplant (supplementary Figure 1, see online at: www.futuremedicine.com/doi/suppl/10.2217/nnm.12.198). FISH analyses demonstrated multiple areas of red fluorescence that correlated to the Y chromosome present in the nuclei of transplanted cells (counterstained by 4',6-diamidino-2-phenylindole:blue) in all implants (Figures 8D–8F & 9D–9F), which corresponded to the presence of Y chromosome-containing transplanted cells in female Sprague–Dawley hosts with an XX genotype.

Discussion

Data showed that ADSCs, labeled with ferumoxytol, could be detected in osteochondral defects of arthritic joints with MRI. Since ferumoxytol is FDA approved as an iron supplement for intravenous treatment of anemias, this nanoparticle compound would be, in principle, readily accessible for *in vivo* tracking of stem-cell transplants in patients via an 'off-label' application [25] .

This study's group and others have shown that the superparamagnetic signal effects of ferumoxytol can be utilized to enhance vessels, visceral organs and various pathologies on MR images [20,41,42]. This study's group was the first to utilize Feraheme as an intravenous contrast agent for MRI of arthritis in an animal model [20] . Following intravenous injection of ferumoxytol, a significant MR signal enhancement was noted of vascular structures [43–45], inflammatory arthritis [20] and tumors [41,46] . To the best of the authors' knowledge, ferumoxytol has not yet been applied for *in vivo* cell-tracking purposes.

Previous studies by the study's group and others used the SPIOs ferumoxides [47, 48] or ferucarbotran [18] for labeling and tracking of human MSCs in arthritic joints. These relatively large SPIOs are spontaneously phagocytosed by stem cells and thus, allow stem-cell labeling via simple incubation [15,17,19,36, 37,47–49] . However, ferumoxides (Endorem and Feridex I.V.) and ferucarbotran (Resovist®, Schering AG, Berlin, Germany) are not produced any more by the pharmaceutical industry. They have also shown to inhibit chondrogenesis in a dose-dependant manner [5,18,50,51]. Instead, ultrasmall SPIOs (USPIOs) are now being produced, which have wider diagnostic applications and improved safety profiles [52] . In addition, this study's data showed that ferumoxytol labeling did not affect chondrogenesis (Figure 5). However, USPIOs are not as efficiently phagocytosed by stem cells as SPIOs and thus, cannot be introduced into target cells via simple incubation protocols. Previous studies demonstrated that the USPIO compounds ferumoxtran-10 (Sinerem® or Combidex® [Guerbet, Aulnay-sous-Bois, France]) and ferucarbotran (Resovist) can be introduced into stem cells using transfections agents such as lipofectine [53] , poly-L-lysine [54, 55] or protamine sulphate [56] . Since ferumoxytol has similar physicochemical characteristics to these USPIOs, an assisted labeling technique was also applied in order to shuttle ferumoxytol into stem cells. Using a modified protocol originally described by Arbab *et al.* [36], ferumoxytol was introduced into stem cells with protamine sulfate as a clinically applicable transfection agent. As shown by the data, the needed concentration for efficient stem-cell labeling with ferumoxytol (500 μg/ml) was much higher compared with ferumoxides (100 μg/ml). This higher concentration of ferumoxytol is needed because of two reasons. First, the smaller size of USPIOs compared with SPIOs leads to lower cellular uptake and lower labeling efficiency of USPIOs compared with SPIOs. Second, the r2 relaxivity (MR signal effect) of USPIOs is markedly lower compared with SPIOs, requiring higher concentrations for MRI detection. A recently published technique by Thu *et al.* demonstrated that ferumoxytol can be introduced into cells by generating ferumoxytol–heparin–protamine complexes [39] . The underlying idea is to create clusters of larger nanoparticles, which are taken up more efficiently by the target

cells. As confirmed by the data from this study, the 'Thu technique' is more efficient than this study's. However, for this study's intended application of transplanting stem cells into injured joints, clinicians requested a 'heparin-free' labeling technique to avoid potential secondary bleeds or heparin-induced cartilage damage [57, 58] . Stem cells have been shown to exocytose their phagocytosed contrast agent *in vivo* [59] . This exocytosis would potentially also affect associated protamine and heparin components. A potential effect of released heparin and heparin–protamine complexes on a local defect milieu has to be investigated in more detail before such a technique could be translated to clinical trials. With this study's protocol, this uncertain effect of heparin does not need to be considered.

Previous studies demonstrated that stem cells labeled with SPIOs, could be tracked in animal models for several weeks [60]. Ferumoxides-labeled MSCs could be tracked in arthritic joints for 7–12 weeks, while ferumoxytol and ferumoxides-labeled ADSCs in this study could be only tracked for approximately 2 weeks. This difference is apparently due to a more rapid cellular proliferation and higher metabolic activity of our rat ADSCs as opposed to hMSCs [61] with consecutive more rapid dilution of iron oxide nanoparticles in ADSCs as opposed to MSCs. In accordance with the observations in this study, Peng *et al.* and Vidal *et al.* also reported a higher proliferation potential and longer time interval to senescence for ADSCs compared with MSCs [26,61]. Bermen *et al.* and Küstermann *et al.* suggested that the metabolization of the iron oxide label and fading signal effect on longitudinal MRI studies can be used as an MR-detectable indicator for the viability of the stem-cell transplant [62,63]. Novel approaches to increase the cellular retention of the ferumoxytol label, in order to provide longer-lasting cell-tracking capabilities with MRI are necessary.

Gadolinium-based MR contrast agents are also FDA approved and can also be introduced into stem cells with the FDA-approved transfection agent protamine sulfate. This study's group and others have reported that stem cells, labeled with clinically approved gadolinium chelates, can be tracked in arthritic joints [64,65]. Thus, gadolinium labeling would represent a potential alternative to ferumoxytol labeling. Advantages of the ferumoxytol approach are: higher sensitivity of the iron oxide label; visualization on proton-density images, typically applied for cartilage evaluation in a clinical setting and; potential for combining direct USPIO cell labeling with intravenous gadolinium injections.

Conclusion

In conclusion, the presented MRI technique allows for direct, noninvasive *in vivo* visualization of transplanted stem cells in MASI. Since an FDA-approved cell label and clinically applicable MRI technology was used in this study, the described technique can, in principle, be readily translated to the evaluation of MASI in patients via an 'off-label' use of ferumoxytol as a cellular label. Employing this technique in the clinic could help to diagnose transplant failures early after stem-cell implantation, avoid invasive follow-up studies and reassign patients with transplant failures to alternate treatment regimens.

Future perspective

The data from this study showed that the iron supplement ferumoxytol can be used as a cell marker for *in vivo* stem-cell tracking with MRI. To the best of the authors' knowledge, ferumoxytol is currently the only FDA-approved iron oxide nanoparticle compound that can be directly translated to the clinic via an 'off-label' application for stem-cell tracking. A limited survival of transplanted stem cells due to mechanical loss, apoptosis or immune rejection is a major barrier for successful tissue regeneration outcomes. As novel stem-cell therapies enter clinical trials, it will be increasingly important to monitor placement,

retention and integration of the transplanted cells into the target tissue. Ferumoxytol-mediated stem-cell tracking will enable us to overcome the bottleneck of diagnosing transplant failures, help to avoid invasive follow-up studies of lost transplants, and aid in assigning patients with transplant failure to early interventions or alternative treatment options.

Supplementary Material

Refer to Web version on PubMed Central for supplementary material.

Acknowledgments

The authors thank J Vancil and G Beck for their excellent help with the creation of the figures for this manuscript.

This work was supported by NIH grant R01AR054458 from the National Institute of Arthritis and Musculoskeletal and Skin Diseases to HE Daldrup-Link and a research stipend from the National University of Singapore to H Nejadnik.

References

Papers of special note have been highlighted as:

' of interest

'' of considerable interest

1. Centers for Disease Control and Prevention. Prevalence of doctor-diagnosed arthritis and arthritis-attributable activity limitation – United States, 2007–2009. MMWR Morb. Mortal. Wkly Rep. 2010; 59(39):1261–1265. [PubMed: 20930703]
2. Centers for Disease Control and Prevention. Arthritis. Meeting the Challenge at a Glance 2011. GA, USA: National Center for Chronic Disease Prevention and Health Promotion; 2011.
3. Hunziker EB. Articular cartilage repair: problems and perspectives. Biorheology. 2000; 37(1–2): 163–164. [PubMed: 10912188]
4. Kinner B, Capito RM, Spector M. Regeneration of articular cartilage. Adv. Biochem. Eng. Biotechnol. 2005; 94:91–123. [PubMed: 15915870]
5. Boddington SE, Sutton EJ, Henning TD, et al. Labeling human mesenchymal stem cells with fluorescent contrast agents: the biological impact. Mol. Imaging Biol. 2011; 13(1):3–9. [PubMed: 20379785]
6. Brittberg M. Autologous chondrocyte transplantation. Clin. Orthop. Relat. Res. 1999; (Suppl. 367):S147–S155. [PubMed: 10546643]
7. Brittberg M, Tallheden T, Sjogren-Jansson B, Lindahl A, Peterson L. Autologous chondrocytes used for articular cartilage repair: an update. Clin. Orthop. Relat. Res. 2001; (Suppl. 391):S337–S348. [PubMed: 11603717]
8. Galle J, Bader A, Hepp P, et al. Mesenchymal stem cells in cartilage repair: state of the art and methods to monitor cell growth, differentiation, cartilage regeneration. Curr. Med. Chem. 2010; 17(21):2274–2291. [PubMed: 20459378]
9. Gao J, Yao JQ, Caplan AI. Stem cells for tissue engineering of articular cartilage. Proc. Inst. Mech. Eng. H. 2007; 221(5):441–450. [PubMed: 17822146]
10. Hunziker EB. Articular cartilage repair: are the intrinsic biological constraints undermining this process insuperable? Osteoarthritis Cartilage. 1999; 7(1):15–28. [PubMed: 10367012]
11. Molcanyi M, Riess P, Bentz K, et al. Trauma-associated inflammatory response impairs embryonic stem cell survival and integration after implantation into injured rat brain. J. Neurotrauma. 2007; 24(4):625–637. [PubMed: 17439346]

12. Li P, Tessler A, Han SS, Fischer I, Rao MS, Selzer ME. Fate of immortalized human neuronal progenitor cells transplanted in rat spinal cord. Arch. Neurol. 2005; 62(2):223–229. [PubMed: 15710850]

13. Bredella MA, Tirman PF, Peterfy CG, et al. Accuracy of T2-weighted fast spin-echo MR imaging with fat saturation in detecting cartilage defects in the knee: comparison with arthroscopy in 130 patients. AJR Am. J. Roentgenol. 1999; 172(4):1073–1080. [PubMed: 10587150]

14. Eckstein F, Reiser M, Englmeier KH, Putz R. *In vivo* morphometry and functional analysis of human articular cartilage with quantitative magnetic resonance imaging – from image to data, from data to theory. Anat. Embryol. Berl. 2001; 203(3):147–173. [PubMed: 11303902]

15. Nedopil A, Klenk C, Kim C, et al. MR signal characteristics of viable and apoptotic human mesenchymal stem cells in matrix-associated stem cell implants for treatment of osteoarthritis. Invest. Radiol. 2010; 45(10):634–640. [PubMed: 20808236]

16. Wang YX. *In vivo* magnetic resonance imaging of animal models of knee osteoarthritis. Lab. Anim. 2008; 42(3):246–264. [PubMed: 18625580]

17. Henning TD, Boddington S, Daldrup-Link HE. Labeling hESCs and hMSCs with iron oxide nanoparticles for noninvasive *in vivo* tracking with MR imaging. J. Vis. Exp. 2008; (13)

18. Henning TD, Sutton EJ, Kim A, et al. The influence of ferucarbotran on the chondrogenesis of human mesenchymal stem cells. Contrast Media Mol. Imaging. 2009; 4(4):165–173. [PubMed: 19670250]

19. Nedopil AJ, Mandrussow LG, Daldrup-Link HE. Implantation of ferumoxides labeled human mesenchymal stem cells in cartilage defects. J. Vis. Exp. 2010; 38:1793. [PubMed: 20368696]

20. Simon GH, Von Vopelius-Feldt J, Fu Y, et al. Ultrasmall supraparamagnetic iron oxide-enhanced magnetic resonance imaging of antigen-induced arthritis: a comparative study between SHU 555 C, ferumoxtran-10 and ferumoxytol. Invest. Radiol. 2006; 41(1):45–51. [PubMed: 16355039] '' Compares different ultrasmall superparamagnetic iron oxides, including ferumoxytol, which was used in this study. Also describes the half-life of ferumoxytol in rodents.

21. Sutton EJ, Henning TD, Boddington S, et al. *In vivo* magnetic resonance imaging and optical imaging comparison of viable and nonviable mesenchymal stem cells with a bifunctional label. Mol. Imaging. 2010; 9(5):278–290. [PubMed: 20868628]

22. Arbab AS, Janic B, Haller J, Pawelczyk E, Liu W, Frank JA. *In vivo* cellular imaging for translational medical research. Curr. Med. Imaging. Rev. 2009; 5(1):19–38. [PubMed: 19768136]

23. Bulte JW. *In vivo* MRI cell tracking: clinical studies. AJR Am. J. Roentgenol. 2009; 193(2):314–325. [PubMed: 19620426]

24. Cromer Berman SM, Walczak P, Bulte JW. Tracking stem cells using magnetic nanoparticles. Wiley Interdiscip. Rev. Nanomed. Nanobiotechnol. 2011; 3(4):343–355. [PubMed: 21472999]

25. Coyne DW. Ferumoxytol for treatment of iron deficiency anemia in patients with chronic kidney disease. Exp. Opin. Pharmacother. 2009; 10(15):2563–2568.

26. Peng L, Jia Z, Yin X, et al. Comparative analysis of mesenchymal stem cells from bone marrow, cartilage and adipose tissue. Stem Cells Dev. 2008; 17(4):761–773. [PubMed: 18393634]

27. Huang JI, Zuk PA, Jones NF, et al. Chondrogenic potential of multipotential cells from human adipose tissue. Plast. Reconstr. Surg. 2004; 113(2):585–594. [PubMed: 14758221]

28. Im GI, Shin YW, Lee KB. Do adipose tissue-derived mesenchymal stem cells have the same osteogenic and chondrogenic potential as bone marrow-derived cells? Osteoarthritis Cartilage. 2005; 13(10):845–853. [PubMed: 16129630]

29. Winter A, Breit S, Parsch D, et al. Cartilage-like gene expression in differentiated human stem cell spheroids: a comparison of bone marrow-derived and adipose tissue-derived stromal cells. Arthritis Rheum. 2003; 48(2):418–429. [PubMed: 12571852]

30. Ning H, Lin G, Lue TF, Lin CS. Neuron-like differentiation of adipose tissue-derived stromal cells and vascular smooth muscle cells. Differentiation. 2006; 74(9–10):510–518. [PubMed: 17177848]

31. Strem BM, Hicok KC, Zhu M, et al. Multipotential differentiation of adipose tissue-derived stem cells. Keio J. Med. 2005; 54(3):132–141. [PubMed: 16237275]

32. Zuk PA, Zhu M, Ashjian P, et al. Human adipose tissue is a source of multipotent stem cells. Mol. Biol. Cell. 2002; 13(12):4279–4295. [PubMed: 12475952]

33. Mitchell JB, Mcintosh K, Zvonic S, et al. Immunophenotype of human adipose-derived cells: temporal changes in stromal-associated and stem cell-associated markers. Stem Cells. 2006; 24(2): 376–385. [PubMed: 16322640]

34. Neuwelt EA, Hamilton BE, Varallyay CG, et al. Ultrasmall superparamagnetic iron oxides (USPIOs): a future alternative magnetic resonance (MR) contrast agent for patients at risk for nephrogenic systemic fibrosis (NSF)? Kidney Int. 2009; 75(5):465–474. [PubMed: 18843256] '' Shows translational potential of ferumoxytol; describes use of intravenously injected ferumoxytol as a contrast agent for MRI in patients.

35. Wang YX, Hussain SM, Krestin GP. Superparamagnetic iron oxide contrast agents: physicochemical characteristics applications in MR imaging. Eur. Radiol. 2001; 11(11):2319–2331. [PubMed: 11702180]

36. Arbab AS, Yocum GT, Kalish H, et al. Efficient magnetic cell labeling with protamine sulfate complexed to ferumoxides for cellular MRI. Blood. 2004; 104(4):1217–1223. [PubMed: 15100158] '' Describes labeling protocols for ferumoxides, which is the basis for the labeling protocol for ferumoxytol in this study.

37. Arbab AS, Yocum GT, Rad AM, et al. Labeling of cells with ferumoxides–protamine sulfate complexes does not inhibit function or differentiation capacity of hematopoietic or mesenchymal stem cells. NMR. Biomed. 2005; 18(8):553–559. [PubMed: 16229060]

38. Castaneda RT, Khurana A, Khan R, Daldrup-Link HE. Labeling stem cells with ferumoxytol, an FDA-approved iron oxide nanoparticle. J. Vis. Exp. 2011; (57):e3482. [PubMed: 22083287]

39. Thu MS, Bryant LH, Coppola T, et al. Self-assembling nanocomplexes by combining ferumoxytol, heparin and protamine for cell tracking by magnetic resonance imaging. Nat. Med. 2012; 18(3): 463–467. [PubMed: 22366951]

40. Wolff SD, Balaban RS. Assessing contrast on MR images. Radiology. 1997; 202(1):25–29. [PubMed: 8988186]

41. Dosa E, Guillaume DJ, Haluska M, et al. Magnetic resonance imaging of intracranial tumors: intra-patient comparison of gadoteridol, ferumoxytol. Neuro. Oncol. 2011; 13(2):251–260. [PubMed: 21163809]

42. Harisinghani M, Ross RW, Guimaraes AR, Weissleder R. Utility of a new bolus-injectable nanoparticle for clinical cancer staging. Neoplasia. 2007; 9(12):1160–1165. [PubMed: 18084623]

43. Li W, Tutton S, Vu AT, et al. First-pass contrast-enhanced magnetic resonance angiography in humans using ferumoxytol, a novel ultrasmall superparamagnetic iron oxide (USPIO)-based blood pool agent. J. Magn. Reson. Imaging. 2005; 21(1):46–52. [PubMed: 15611942]

44. Neuwelt EA, Varallyay CG, Manninger S, et al. The potential of ferumoxytol nanoparticle magnetic resonance imaging, perfusion, and angiography in central nervous system malignancy: a pilot study. Neurosurgery. 2007; 60(4):601–611. discussion 611–612. [PubMed: 17415196]

45. Ersoy H, Jacobs P, Kent CK, Prince MR. Blood pool MR angiography of aortic stent–graft endoleak. AJR Am. J. Roentgenol. 2004; 182(5):1181–1186. [PubMed: 15100115]

46. Gahramanov S, Raslan AM, Muldoon LL, et al. Potential for differentiation of pseudoprogression from true tumor progression with dynamic susceptibility-weighted contrast-enhanced magnetic resonance imaging using ferumoxytol vs. gadoteridol: a pilot study. Int. J. Radiat. Oncol. Biol. Phys. 2011; 79(2):514–523. [PubMed: 20395065]

47. Farrell E, Wielopolski P, Pavljasevic P, et al. Effects of iron oxide incorporation for long term cell tracking on MSC differentiation*in vitro* and *in vivo* . Biochem. Biophys. Res. Commun. 2008; 369(4):1076–1081. [PubMed: 18336785]

48. Henning TD, Gawande R, Khurana A, et al. Magnetic resonance imaging of ferumoxide-labeled mesenchymal stem cells in cartilage defects: *in vitro* and *in vivo* investigations. Mol. Imaging. 2011; 11(3):197–209. [PubMed: 22554484] '' Study by the authors of this article's group that describes long-term tracking of iron oxide-labeled human mesenchymal stem cells in arthritic joints with MRI, using the 'frst-generation' clinical iron oxide nanoparticle compound ferumoxides. Ferumoxides are not available any more; the second-generation ultrasmall superparamagnetic iron oxide ferumoxytol is now used as an alternative cell label.

49. Wang L, Deng J, Wang J, et al. Superparamagnetic iron oxide does not affect the viability and function of adipose-derived stem cells, and superparamagnetic iron oxide-enhanced magnetic

resonance imaging identifies viable cells. Magn. Reson. Imaging. 2009; 27(1):108–119. [PubMed: 18657922]

50. Bulte JW, Kraitchman DL, Mackay AM, Pittenger MF. Chondrogenic differentiation of mesenchymal stem cells is inhibited after magnetic labeling with ferumoxides. Blood. 2004; 104(10):3410–3413. [PubMed: 15525839]
51. Kostura L, Kraitchman DL, Mackay AM, Pittenger MF, Bulte JW. Feridex labeling of mesenchymal stem cells inhibits chondrogenesis but not adipogenesis or osteogenesis. NMR Biomed. 2004; 17(7):513–517. [PubMed: 15526348]
52. Lu M, Cohen MH, Rieves D, Pazdur R. FDA report: ferumoxytol for intravenous iron therapy in adult patients with chronic kidney disease. Am. J. Hematol. 2010; 85(5):315–319. [PubMed: 20201089]
53. Daldrup-Link HE, Rudelius M, Oostendorp RA, et al. Targeting of hematopoietic progenitor cells with MR contrast agents. Radiology. 2003; 228(3):760–767. [PubMed: 12881578]
54. Babic M, Horak D, Trchova M, et al. Poly(l-lysine)-modified iron oxide nanoparticles for stem cell labeling. Bioconjug. Chem. 2008; 19(3):740–750. [PubMed: 18288791]
55. Xu Q, Zhang HT, Liu K, et al. *In vitro* and *in vivo* magnetic resonance tracking of Sinerem-labeled human umbilical mesenchymal stromal cell-derived Schwann cells. Cell. Mol. Neurobiol. 2011; 31(3):365–375. [PubMed: 21120599]
56. Wu YJ, Muldoon LL, Varallyay C, Markwardt S, Jones RE, Neuwelt EA. *In vivo* leukocyte labeling with intravenous ferumoxides/protamine sulfate complex *in vitro* characterization for cellular magnetic resonance imaging. Am. J. Physiol. Cell Physiol. 2007; 293(5):C1698–C1708. [PubMed: 17898131]
57. Roosendaal G, Vianen ME, van den Berg HM, Lafeber FP, Bijlsma JW. Cartilage damage as a result of hemarthrosis in a human *in vitro* model. J. Rheumatol. 1997; 24(7):1350–1354. [PubMed: 9228136]
58. Brown CC, Balian G. Effect of heparin on synthesis of short chain collagen by chondrocytes, smooth muscle cells. J. Cell. Biol. 1987; 105(2):1007–1012. [PubMed: 3114266]
59. Cromer Berman SM, Kshitiz Wang CJ, et al. Cell motility of neural stem cells is reduced after SPIO-labeling, which is mitigated after exocytosis. Magn. Reson. Med. 2012; 69(1):255–262. [PubMed: 22374813]
60. Kraitchman DL, Heldman AW, Atalar E, et al. *In vivo* magnetic resonance imaging of mesenchymal stem cells in myocardial infarction. Circulation. 2003; 107(18):2290–2293. [PubMed: 12732608]
61. Vidal MA, Walker NJ, Napoli E, Borjesson DL. Evaluation of senescence in mesenchymal stem cells isolated from equine bone marrow, adipose tissue, and umbilical cord tissue. Stem Cells Dev. 2011; 21(2):273–283. [PubMed: 21410356] ▪ Reported a higher proliferation potential and longer time interval to senescence for adipose-derived stem cells compared with mesenchymal stem cells, which could explain the faster dilution of iron oxides and related signal effects in this study compared with previous imaging studies by this study's group and others.
62. Berman SC, Galpoththawela C, Gilad AA, Bulte JW, Walczak P. Long-term MR cell tracking of neural stem cells grafted in immunocompetent versus immunodeficient mice reveals distinct differences in contrast between live and dead cells. Magn. Reson. Med. 2011; 65(2):564–574. [PubMed: 20928883]
63. Küstermann E, Himmelreich U, Kandal K, et al. Efficient stem cell labeling for MRI studies. Contrast Media Mol. Imaging. 2008; 3(1):27–37. [PubMed: 18335477]
64. Saborowski O, Simon GH, Raatschen HJ, et al. MR imaging of antigen-induced arthritis with a new, folate receptor-targeted contrast agent. Contrast Media Mol. Imaging. 2007; 2(2):72–81. [PubMed: 17385788]
65. Anderson SA, Lee KK, Frank JA. Gadolinium-fullerenol as a paramagnetic contrast agent for cellular imaging Invest. Radiol. 2006; 41(3):332–338.

Executive summary

***In vitro* studies**

- Ferumoxytol-labeled adipose-derived stem cells (ADSCs) demonstrated significantly shortened T2 relaxation times compared with unlabeled ADSCs ($p < 0.05$).
- A labeling protocol with 500 μg iron/ml ferumoxytol and 10 μg/ml protamine sulfate was considered the best compromise between significant magnetic resonance signal, maximal iron uptake and preserved viability of labeled ADSCs.

***In vivo* studies**

- Labeled and unlabeled matrix-associated stem-cell implants demonstrated significantly different signal-to-noise ratios on T2-weighted magnetic resonance images ($p < 0.01$).
- At 4 weeks, signal-to-noise ratio data of labeled ADSCs (both ferumoxytol and ferumoxides) were back to baseline. A FISH analysis confirmed engraftment of both labeled and unlabeled ADSCs in osteochondral defects. Histopathology confirmed slow dilution of the iron oxide label over time.

Discussion

- ADSCs can be labeled with the US FDA-approved iron supplement ferumoxytol and protamine sulfate. This technique would be, in principle, readily clinically applicable via an ‘off-label’ use of these agents.
- Employing this stem-cell imaging technique in patients with matrix-associated stem cell implants could help to diagnose transplant failures early after stem-cell implantation with noninvasive imaging tests, avoid invasive follow-up studies and reassign patients with transplant failures to alternate treatment regimens.

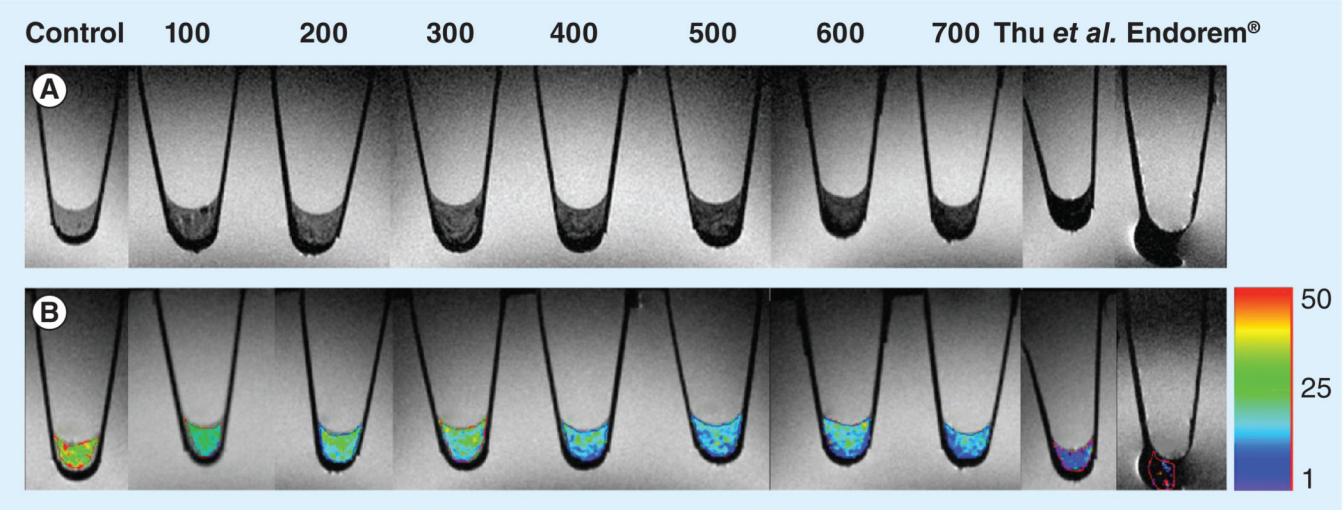

Figure 1. Magnetic resonance signal effects of ferumoxytol-labeled stem cells

(A) T2-weighted magnetic resonance images and **(B)** T2 relaxation time maps of centrifuged stem-cell pellets, labeled with increasing concentrations of ferumoxytol (μg/ml). Labeled cell pellets show a marked negative signal (dark) compared with unlabeled controls. Endorem® (Guerbet, Aulnay-sous-Bois, France; ferumoxides, 100 μg/ml) and ferumoxytol samples, labeled according to Thu *et al.* [39], shown for comparison.

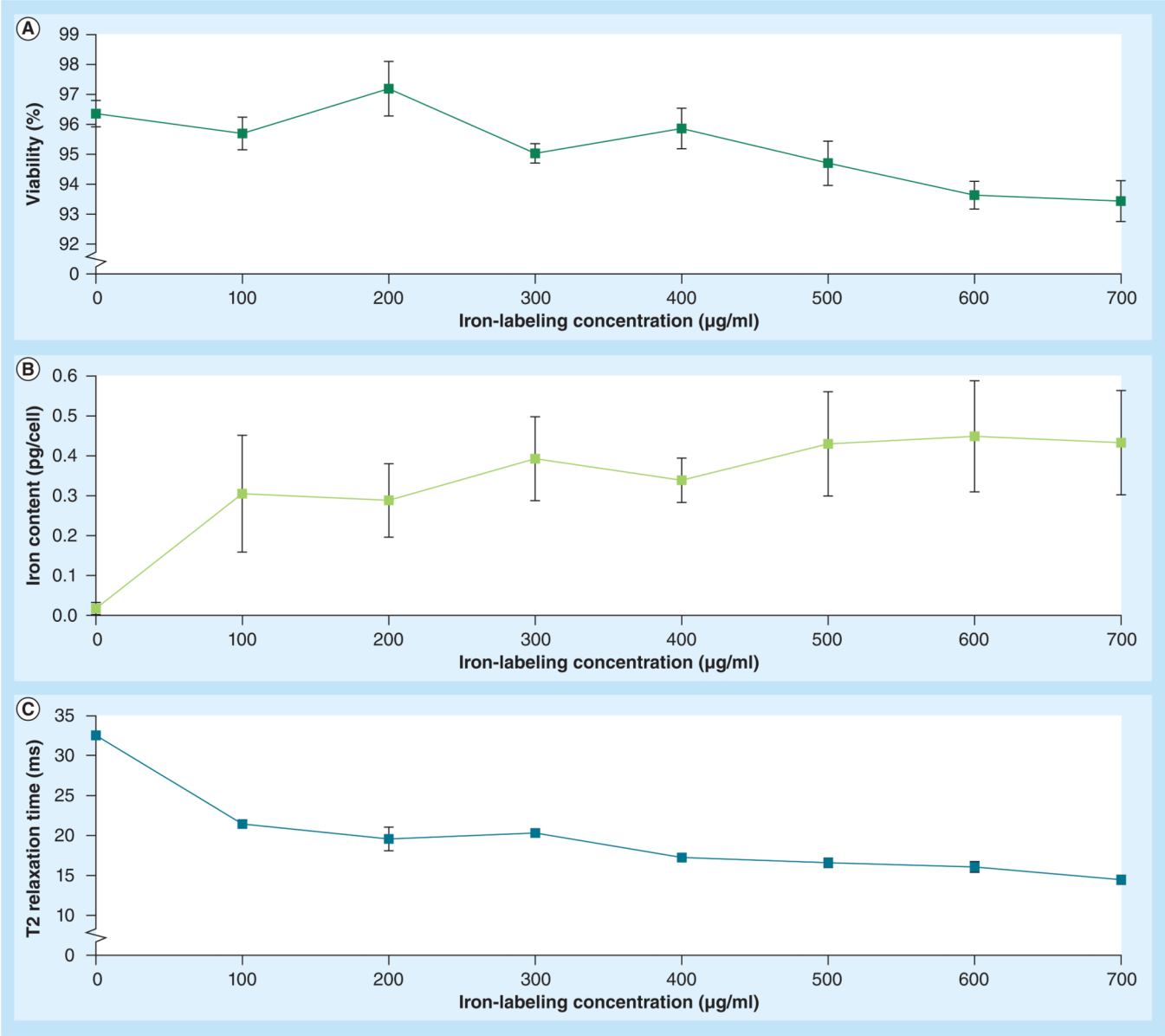

Figure 2. *In vitro* evaluations of ferumoxytol-labeled cells

(A) Viability, **(B)** iron content and **(C)** T2 relaxation time of stem cells, labeled with increasing concentrations of ferumoxytol. Data are displayed as means and standard errors of triplicate samples per experimental group, with 0.5×10^6 cells per sample.

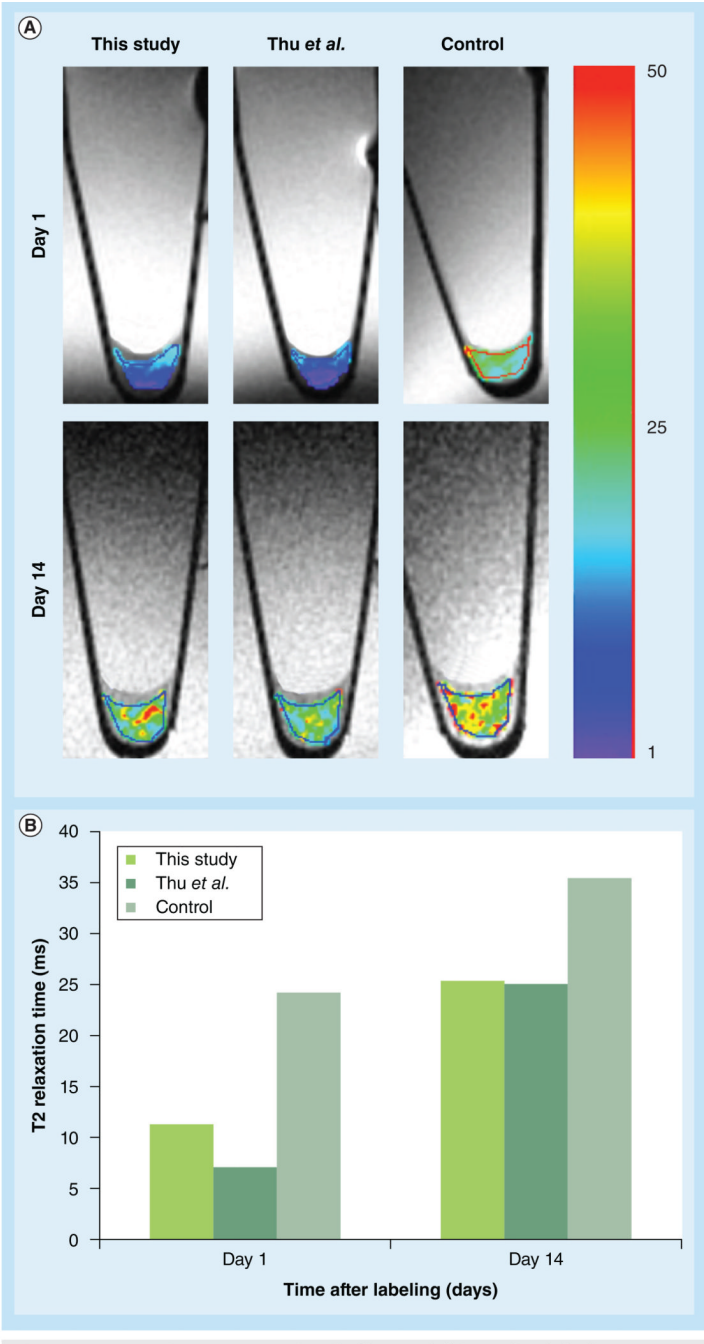

Figure 3. Magnetic resonance signal effects of this study's labeling technique compared with Thu *et al*.'s over time

(A) T2 relaxation time maps of stem-cell pellets, labeled with this study's technique, Thu *et al.*'s technique [39] and control samples at days 1 and 14 post labeling along with **(B)** corresponding graph of mean T2 relaxation times and standard errors of triplicate samples per experimental group, showing no difference in T2 relaxation times between this study's and Thu *et al.*'s technique [39] after 14 days post labeling.

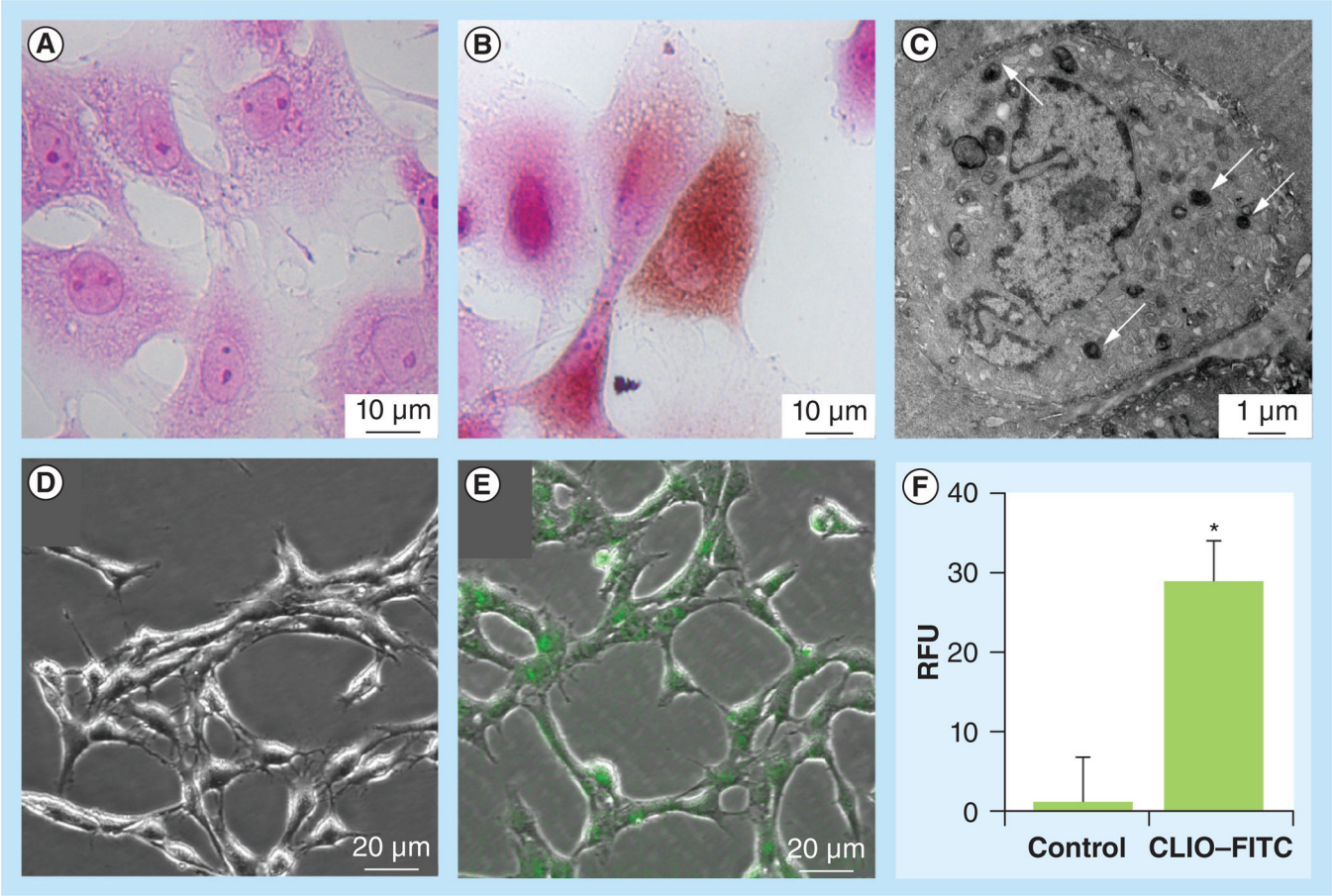

Figure 4. Ferumoxytol uptake by adipose-derived stem cells

3,3′-diaminobenzidine–Prussian blue stains of **(A)** unlabeled control cells and **(B)** ferumoxytol-labeled cells. **(C)** Transmission electron microscopy image of an adipose-derived stem cell labeled with 500 μg/ml ferumoxytol showing iron nanoparticles in secondary lysosomes in the cytoplasm (arrows). **(D)** Fluorescence microscopy of unlabeled control cells and **(E)** FITC-conjugated ferumoxytol labeled cells. Only ferumoxytol-labeled cells demonstrate positive 3,3′-diaminobenzidine–Prussian blue staining and positive fluorescence. **(F)** Mean fluorescence per cell, as quantified in a Cell-IQ® 2 imager (Chip-Man Technologies Ltd, Tempere, Finland), of triplicate samples per experimental group with standard deviations.

*Indicates significant differences between unlabeled controls and FITC-conjugated ferumoxytol-labeled cells ($p < 0.05$).

CLIO: Cross-linked iron oxide; FITC: Fluorescein isothiocyanate; RFU: Relative fluorescence unit.

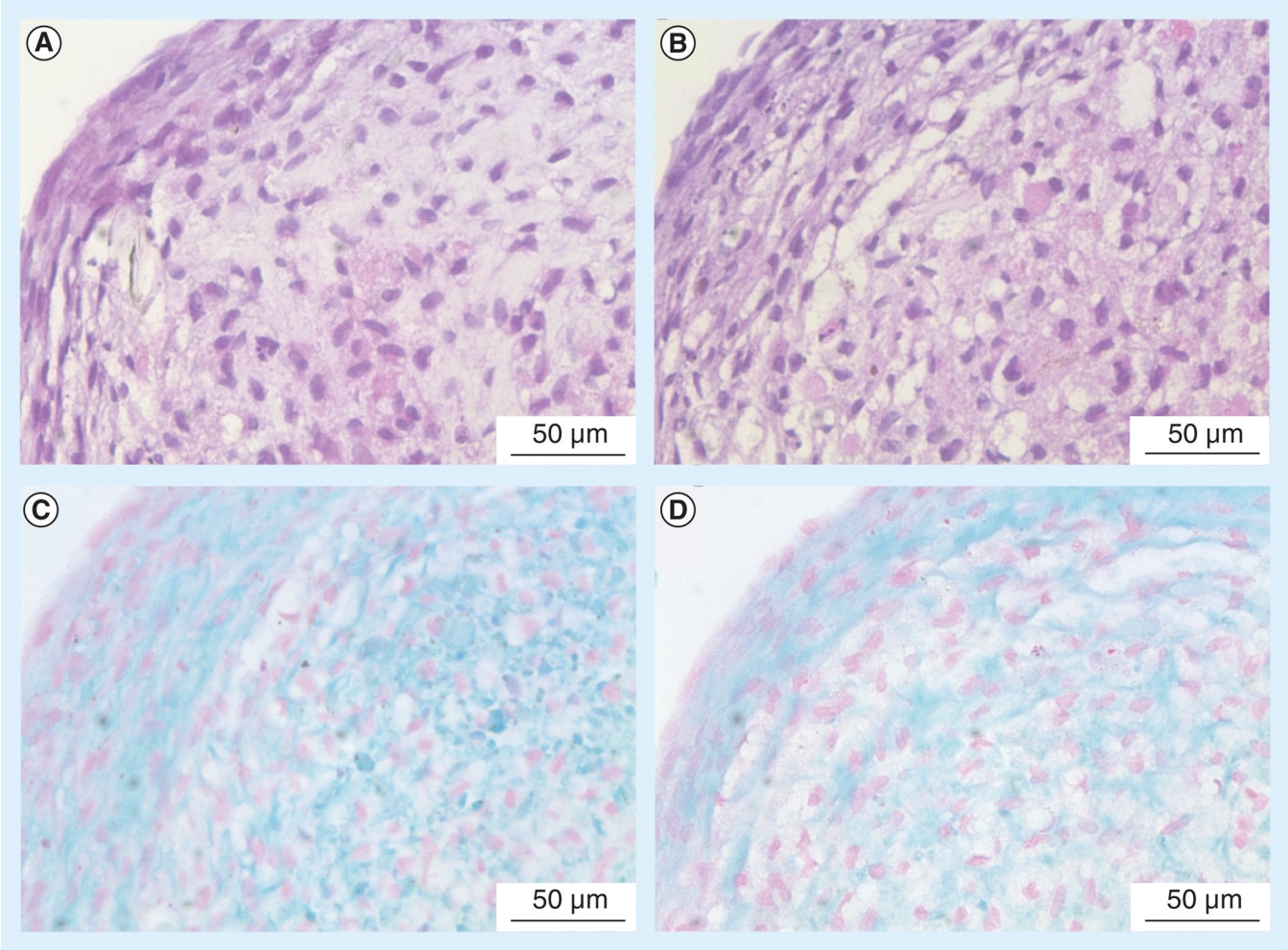

Figure 5. Chondrogenic differentiation of control and labeled cell pellets

(A) Hematoxylin and eosin stain of control and **(B)** labeled cell pellets are shown. **(C)** Alcian blue stains of control and **(D)** labeled cells showing positive (blue) staining, suggesting uninhibited chondrogenesis.

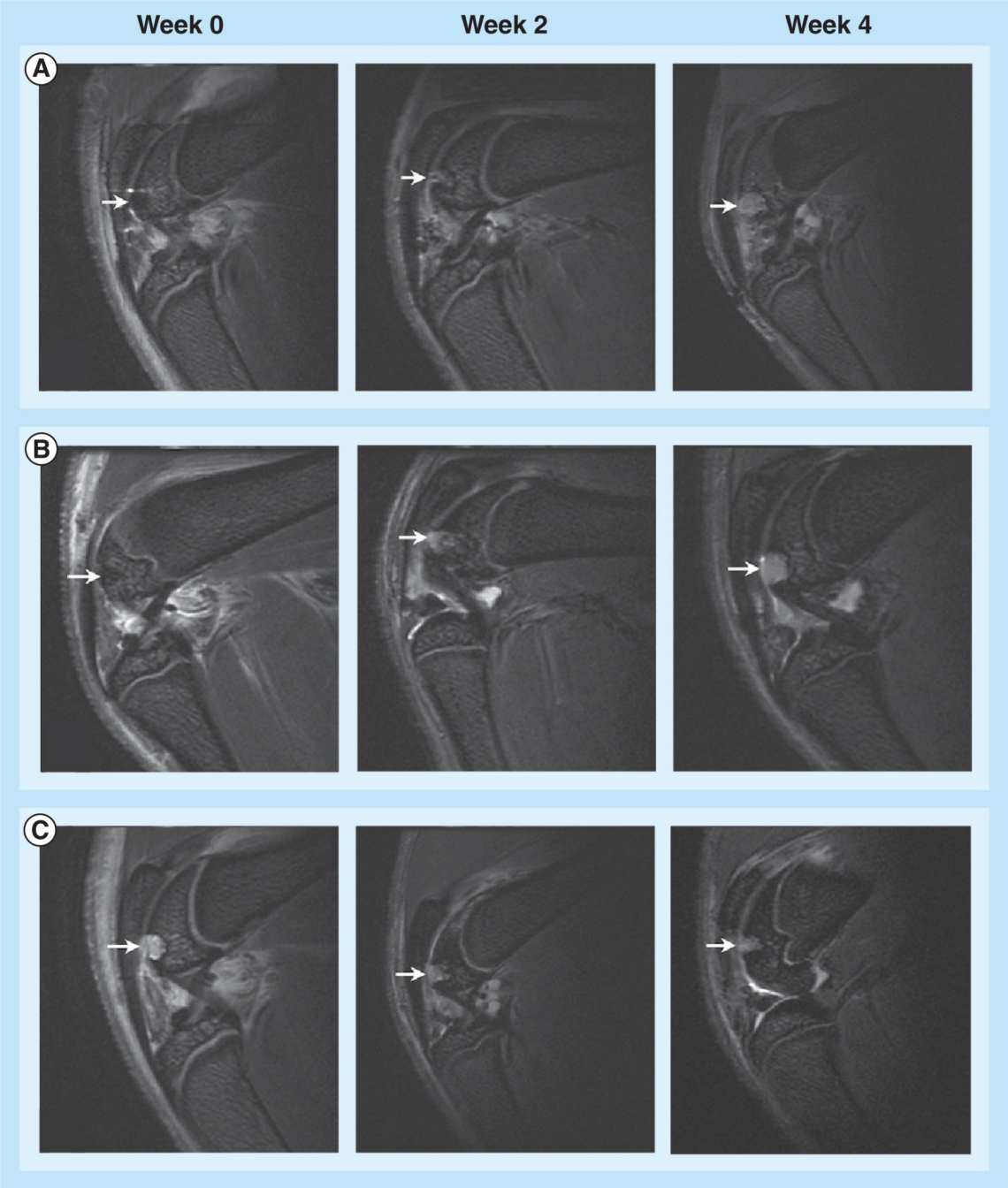

Figure 6. Sagittal T2-weighted magnetic resonance images through representative knee joints with matrix-associated stem-cell transplants (arrows) in osteochondral defects of the distal femur

(A) Ferumoxytol-labeled cell transplants, **(B)** ferumoxides-labeled cell transplants and **(C)** unlabeled controls at week 0, 2 and 4 post-adipose-derived stem-cell implantation. Ferumoxytol- and ferumoxides-labeled cell transplants demonstrate a strong, negative signal effect *in vivo*, which slowly declines over time. Field of view was 2.5 × 2.5 cm.

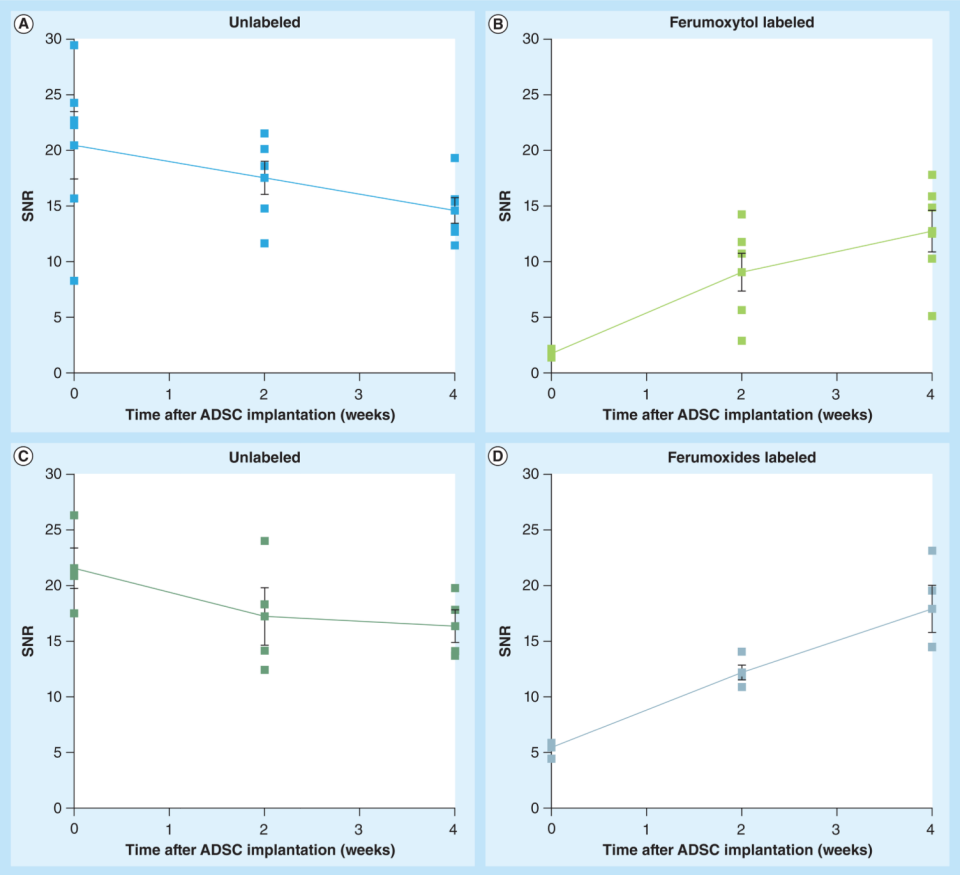

Figure 7. Corresponding quantitative magnetic resonance signal effects of labeled and unlabeled matrix-associated stem-cell transplants *in vivo*

(A & C) SNRs of unlabeled cell transplants: **(A)** n = 6; **(C)** n = 4, showing unchanged signal over 4 weeks. SNRs of **(B)** ferumoxytol-labeled (n = 6) and **(D)** ferumoxides-labeled stem-cell transplants (n = 4), showing slow decline of signal (increase in SNR) over 4 weeks, suggesting slow dilution of the iron label. The SNR is significant between ferumoxytol-labeled and unlabeled cell transplants until week 2 and not significant between ferumoxytol- and ferumoxides-labeled cell transplants at all time points. Data are displayed as mean SNRs and standard errors of ferumoxytol-labeled ADSCs (n = 6) or ferumoxides-labeled ADSCs (n = 4) and corresponding unlabeled controls (n = 10) at different time points after stem-cell implantation.

ADSC: Adipose-derived stem cell; SNR: Signal-to-noise ratio.

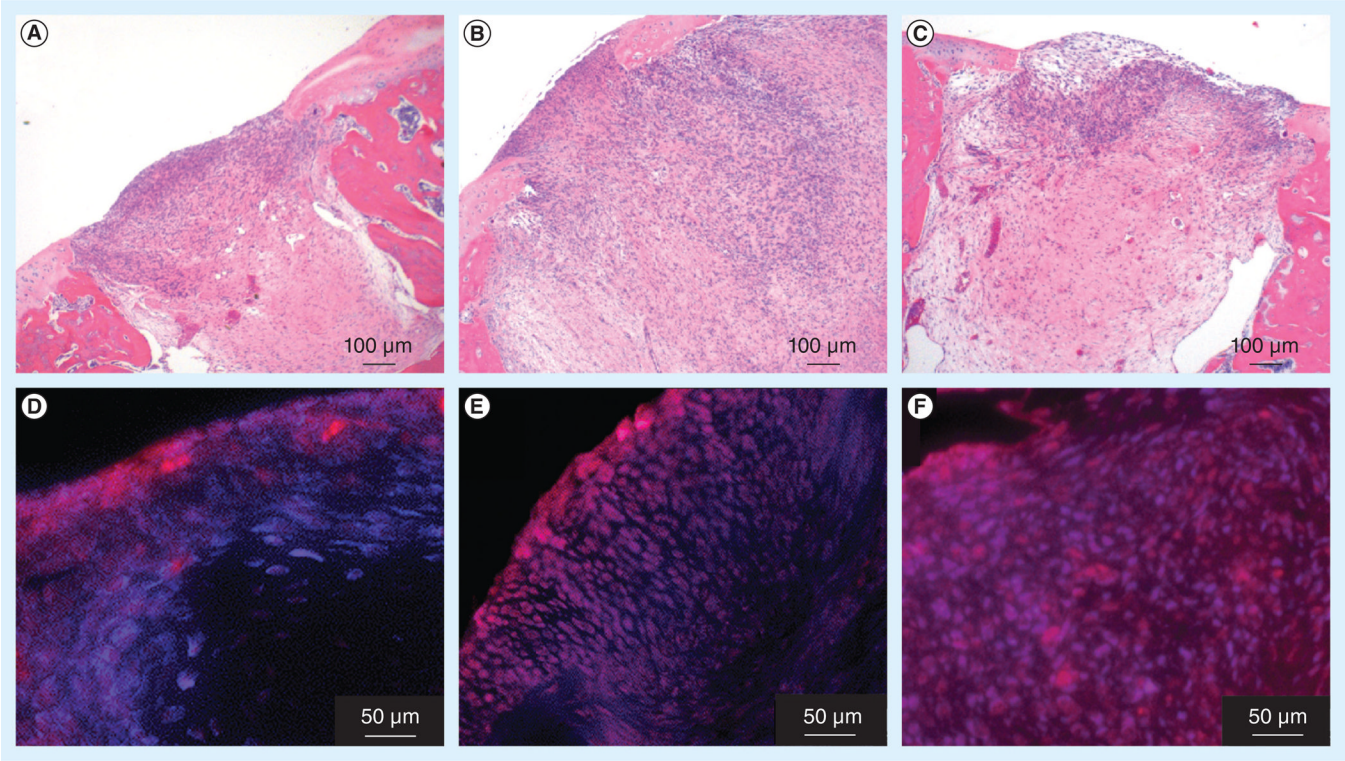

Figure 8. Histopathologic correlations of *in vivo* MRI data

Hematoxylin and eosin stains of **(A)** unlabeled controls showing engraftment of both labeled and unlabeled adipose-derived stem cells in the defect. **(B)** Ferumoxytol- and **(C)** ferumoxides-labeled matrix-associated stem-cell implant at 4 weeks after transplantation. FISH stains against rat Y chromosome showing red fluorescence localized to the nuclei of transplanted cells (counterstained by 4′,6-diamidino-2-phenylindole:blue) in all implants (**[D]** control, **[E]** ferumoxytol-labeled and **[F]** ferumoxides-labeled) suggesting transplanted XY cells in XX female rats.

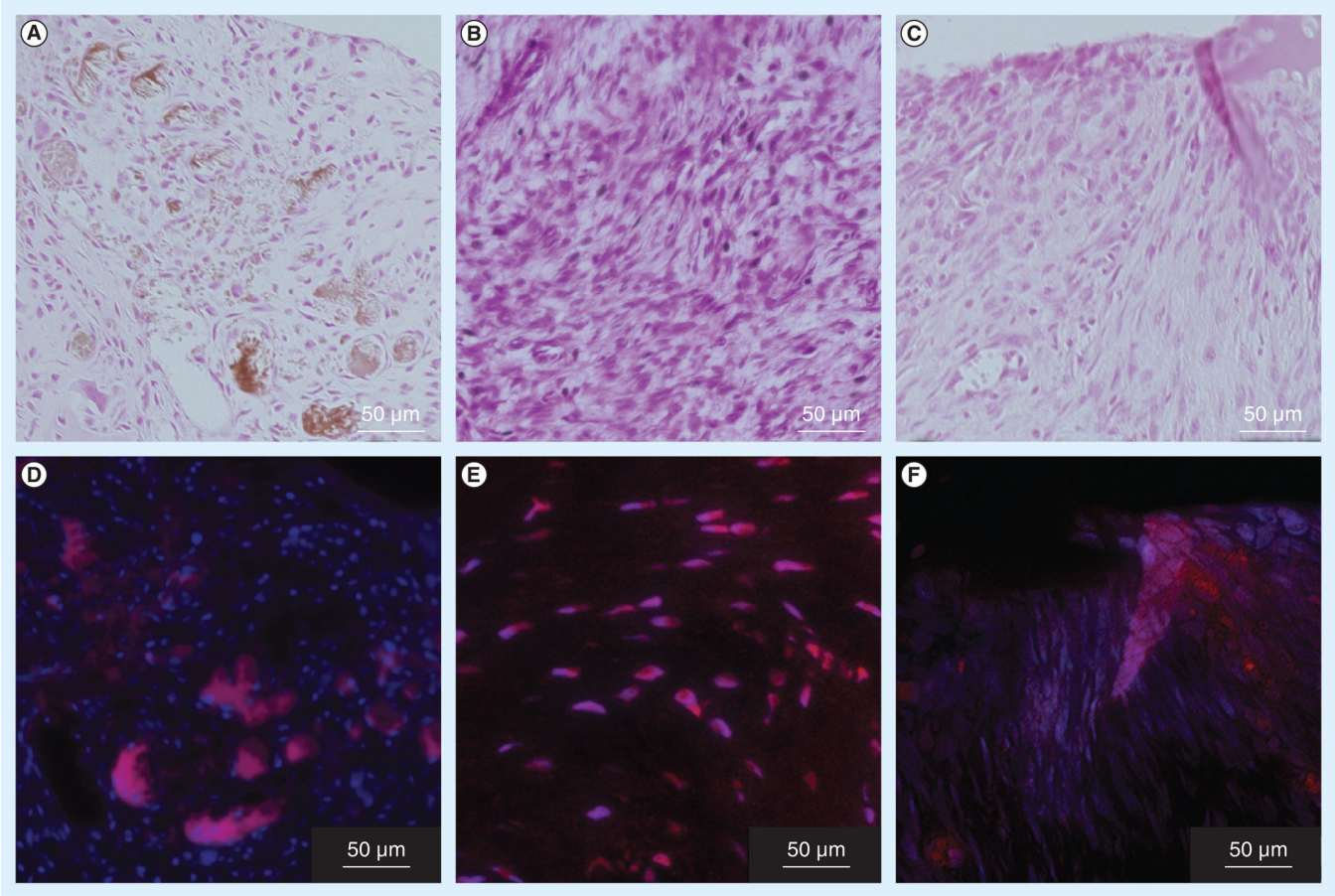

Figure 9. Histologic correlation of iron and FISH stains in stem-cell transplants

Positive 3,3′-diaminobenzidine–Prussian blue staining (brown) is seen at 2 weeks after transplantation in **(A)** ferumoxytol-labeled adipose-derived stem cells but not at **(B)** 4-weeks post-transplant showing slow dilution of iron oxide label over time. **(C)** Unlabeled controls remain unstained. FISH stains against rat Y chromosome showing red fluorescence localized to the nuclei of transplanted cells (counterstained by 4′,6-diamidino-2-phenylindole:blue) at both **(D)** 2-week and **(E)** 4-week post-implant along with **(F)** unlabeled implants demonstrating transplanted XY cells in XX female rats.